Simulation of loss mechanisms in organic solar cells: A description of the mesoscopic Monte Carlo technique and an evaluation of the first reaction method

Chris Groves,[1,a)] Robin G. E. Kimber,[2] and Alison B. Walker[2,b)]
[1]*School of Engineering and Computing Science, Durham University, South Road, Durham DH1 3LE, United Kingdom*
[2]*Department of Physics, University of Bath, Bath BA2 7AY, United Kingdom*

(Received 5 June 2010; accepted 26 July 2010; published online 13 October 2010)

In this letter we evaluate the accuracy of the first reaction method (FRM) as commonly used to reduce the computational complexity of mesoscale Monte Carlo simulations of geminate recombination and the performance of organic photovoltaic devices. A wide range of carrier mobilities, degrees of energetic disorder, and applied electric field are considered. For the ranges of energetic disorder relevant for most polyfluorene, polythiophene, and alkoxy poly(phenylene vinylene) materials used in organic photovoltaics, the geminate separation efficiency predicted by the FRM agrees with the exact model to better than 2%. We additionally comment on the effects of equilibration on low-field geminate separation efficiency, and in doing so emphasize the importance of the energy at which geminate carriers are created upon their subsequent behavior.
 [doi:10.1063/1.3483603]

I. INTRODUCTION

Organic photovoltaic devices (OPVs) made from solution-processable materials can make use of potentially low-cost manufacture techniques, and as such may prove to be a new paradigm in the generation of renewable energy. The efficiencies of OPVs currently lag behind their inorganic counterparts and must be improved if they are to be successfully commercialized. This is complicated by the seemingly unavoidable need of a bulk heterojunction (BHJ) for efficient charge generation in OPVs.[1,2] The formation of a BHJ is in itself rather straightforward, since one only needs to cast a film from a common solution of the two materials with differing electron affinities. For optimal OPV performance we require the domains of the BHJ to be around the exciton diffusion length[3,4] of ~10 nm.[5] While this can be broadly achieved by altering the manufacture conditions,[6,7] the BHJ invariably shows significant heterogeneity in morphology and as such heterogeneity in performance.[8] Since the performance of OPVs is inextricably linked to morphology, and the morphology can be complicated, this poses the question of how one goes about modeling to understand their operation, and ultimately provide guidance as to how they can be improved.

As one might expect there is a wide spectrum of modeling techniques for examining charge transport and device performance,[9–12] each of which can be useful in different circumstances. Since morphology is key to determining the performance of OPVs, a model that includes the effect of morphology without being computationally expensive desirable. A popular technique to achieve this is mesoscopic Monte Carlo (MMC). In MMC the tangled polymer chains and small molecules are simplified into a Cartesian grid, the cells of which that has either electron- or hole-transporting character. As a result, information as to the effect of, for example chain rotation,[13] may be lost, but generic properties of the transporting materials such as energetic disorder and average coupling constant between hopping sites are retained. Most importantly, information relating to the nanoscale morphology can be included. This balance of capabilities is particularly appropriate to OPVs and has already been used to show the effect of morphology on open-circuit voltage, short-circuit current, and device efficiency.[14–17] MMC models are able to reproduce key findings of experimental data including, for example, the Poole–Frenkel type electric field dependence of carrier mobility,[15] the importance of geminate recombination[14–16,18] as seen in polymer-polymer[4,19] and polymer-fullerene[20,21] OPVs, and the effect of morphology on OPV performance[14–16,22] as reported widely in experiment.[8] Furthermore, MMC models have allowed close examination of important aspects of OPV performance such as geminate[22–25] and bimolecular[15,26] recombination, mobility,[27] and exciton dissociation.[14,16] MMC models have allowed examination of the impact of specific physical processes or device geometries upon OPV performance, such as charge trapping,[18] high on/off chain mobility ratios,[25] and bicontinuous gyroid morphologies,[3] which would be difficult to achieve experimentally. Thus, while having its drawbacks, the MMC model has proven itself to be a useful tool in analyzing the performance of OPVs.

However, MMC models are only barely feasible for the simulation of OPV characteristics even when multiple processor supercomputers are used. This is because the number of charges considered is typically in the range of 100, and for each carrier one must calculate all of the possible hopping and recombination events in a morphologically and energeti-

[a)]Electronic mail: chris.groves@durham.ac.uk.
[b)]Electronic mail: a.b.walker@bath.ac.uk.

cally disordered landscape. Furthermore, the simulation must be allowed to proceed for a sufficiently long time to obtain reliable average values. A key simplification to allow these simulations to be possible is the so-called first reaction method (FRM).[28] The FRM relates to how the hopping behavior of the charges is calculated, and so before discussing the FRM in detail, we will first review the important considerations with regard to charge transport in a device. The rate of charge hopping depends upon the associated change in potential. In conjugated polymers and small molecules the dielectric constant is low ($\varepsilon \sim 3-4$), meaning that charges experience a strong Coulombic interaction with carriers in their local vicinity. These charges are mobile, and so the potential landscape is constantly fluctuating. In an exact simulation, the behavior of all charges would be updated whenever the potential landscape changed, for example when a carrier hops or recombines. Constantly updating the behavior of all carriers after any event in the simulation makes it unfeasible to simulate OPV characteristics. In the FRM method, the behavior of each charge is calculated once when a charge is moved to a particular location and *not* updated when the local potential landscape changes. As number of carriers in an OPV simulation is of the order ~ 100 (with variations depending on morphology and incident light intensity), the FRM saves a factor of ~ 100 in run-time compared to the exact simulation. When one considers that even an FRM simulation of an OPV *J-V* curve takes of the order 10 h on a supercomputing cluster, it soon becomes apparent the exact method carries an almost prohibitive computational burden. In addition to the significant savings in run-time, the FRM framework allows easy avoidance of the pitfalls associated with "double counting" of recombination events, which will be discussed further in Sec. II.

One might expect the FRM to become a bad approximation to the exact method in circumstances when the local potential changes by large amounts quickly. This is a circumstance that occurs often in the process of geminate recombination or separation, as photogenerated geminate charges are tethered Coulombically to one another either side of the interface between electron- and hole-transport materials and make repeated (often unsuccessful) attempts to separate on short time scales prior to recombination,[3,22] unless the carriers are trapped.[18] The only test to date on the validity of the FRM examined the dynamic behavior of geminate charges when both electron and hole mobilities were equal,[15] in which it was found the FRM and exact method agreed well. However the absolute effect of the FRM on the geminate separation efficiency, η_{GS}, has not been measured, nor has the effect of differing carrier mobilities or energetic disorder. The uncertainty surrounding the accuracy of the FRM has led some authors[26,29] to use the exact method when perhaps the extra computational expense is unnecessary. Since geminate recombination has been identified as a major loss mechanism in OPVs,[4,19–21] it is crucial that the accuracy of MMC models using the FRM technique is established.

Hence, in this paper we test the validity of the FRM method when compared to the exact method in the simulation of geminate separation efficiency over a wide range of circumstances that are relevant for OPVs. The data presented here were generated by two realizations of the MMC code that have been developed in isolation of one another allowing us to also comment on the portability of MMC techniques discussed here. Furthermore, since we have generated data for the purposes of comparison over a wide field range, we are able to comment on low-field geminate separation efficiency, which is important in determining the open-circuit voltage of OPVs.

II. SIMULATION METHODOLOGY

As is common in MMC models, the morphology is here represented by a regularly spaced Cartesian array of sites that have either electron- or hole-transporting character, which we will denote as material A and B, respectively. Blend morphologies are generated using the simulated annealing approach of Peumans *et al.*[30] In this technique, each site is initially randomly assigned to be either A or B with a probability that corresponds to the blend ratio, which here is 1:1. A pair of adjacent sites is then chosen at random and the change in interfacial energy associated with the pair swapping positions, ΔE, is calculated. To ensure that phase separation is energetically favored we must satisfy $2E_{AB}-E_{AA}-E_{BB} \geq 0$, and so here we choose

$$2E_{AB} = E_{AA} = E_{BB}. \tag{1}$$

Pairwise swaps are accepted with probability

$$P(\Delta E) = \frac{\exp(-\Delta E/kT)}{1+\exp(-\Delta E/kT)}. \tag{2}$$

Many attempts at pairwise swaps are made until one obtains the desired domain size, d. By assuming the morphology to be a regular array of cubes, one can estimate d from the blend volume V and interfacial area A

$$d = \frac{3V}{A}. \tag{3}$$

Typically $\sim 10^6$ iterations are required to obtain morphologies that are of the length scale of ~ 10 nm if the lattice spacing is 1 nm, as is the case here. The simulated annealing approach of generating morphology reproduces some of the features seen in real devices, especially those in small-molecule systems. Other techniques have also been used in MMC models that allow the inclusion of more information, for example the "slithering snake" approach[25,31] allows description of chain positions, whereas more complete descriptions of polymer phase-separation dynamics[32] allow description of heterogeneity on multiple length scales. Here we are interested in examining the behavior of geminate pair separation as predicted by the FRM and exact methods and so we will consider bilayers, as they are the simplest test system, and $d=10$ nm blend morphologies, since this is appropriate to OPV devices.

After the morphology is generated, each site is assigned a Gaussian distributed energy to mimic the effects of energetic disorder. The standard deviation of the distribution, σ, is varied over the range of 0–150 meV to encompass the range of values of energetic disorder commonly reported for conjugated polymers used in OPVs.[33–35] A simulation begins

by the introduction of a geminate pair to a randomly chosen pair of sites that comprise either side of a heterojunction. Implicit in this assumption is that charges are created uniformly within the density of states of the highest occupied molecular orbital and lowest unoccupied molecular orbital, an assumption that has been made by a number of authors.[15,22,23] However, recently it has been shown that the energy of the site which the geminate pair created can have a dramatic effect on its eventual separation efficiency.[18] This has implications for the simulation of OPVs, since exciton migration will lead to geminate charges being created at lower energies in the density of states, and so including the effects of exciton migration is likely to be important in simulating real OPV devices.[14] However, since it is difficult to define an energy at which charges are injected that is universally applicable, and our prime purpose is to test the method rather than further explore the physical process of charge separation, we make the assumption that charges are injected randomly within the density of states. We discuss in Sec. IV the effect of this assumption on low field dissociation probability. Returning to the simulation methodology, charges can recombine when adjacent at a constant rate, which here is taken to be 10^7 s^{-1}. Carriers can also move by nearest neighbor hops from their current site, i to nearest neighbor sites of the appropriate material (electrons to A, holes to B), j at a rate described by the Marcus equation

$$w_{ij} = N_{e(h)} \upsilon \exp\left(- \frac{(E_j - E_i + E_R)^2}{4E_R \ kT} \right), \tag{4}$$

where υ is a factor that describes the average inter- and intramolecular coupling that is assumed to be 10^{11} s^{-1},[18] E_j and E_i are the site energies, while E_R is the reorganization energy associated with electron- or hole-transfer which for this reaction is twice the polaron energy and taken to be 0.25 eV.[18] $N_{e(h)}$ is a prefactor to modify the mobility of the electron (hole), which is 1 unless otherwise specified. Site energies include Coulomb interactions between carriers, assuming a relative dielectric constant of 4, and the contribution from energetic disorder with a Gaussian distribution of width σ noted above.

Additionally, it is worth noting that in device models the question of how to include Coulomb interactions between charges and image charges is a very important one. In early models[14,15] Coulomb interactions were calculated by use of a potential array that had the same dimensions as the morphology. Whenever a charge was introduced or removed, this potential array was modified by the monopole potential of the charge, and whenever a charge was moved the potential array was modified by a dipole potential. The potential array could then be used as a reference to calculate the hopping rates of carriers, while paying careful attention to ensure that the potential due to the carrier under consideration was corrected for in the calculation. To include all Coulombic interactions would mean modifying every element in the potential array whenever an event occurred in the simulation. Practically speaking this is too time consuming, since perhaps 10^6 potentials within the array would have to be altered any time an event within the simulation occurred. The early way of coping with this was to introduce a cut-off radius r_c beyond which Coulombic interactions would not be included. Depending upon the value of r_c chosen, which varied from the Coulomb capture radius ($\sim$16 nm)[15] to some multiple of the Debye length ($\sim$9 nm),[14] the number of potentials needing to be updated dropped by factors between 30 and 170 when compared to the exact method. Recently Casalegno *et al.*[29] evaluated the impact of the cut-off radius approximation on simulated OPV performance by comparison to an exact and computationally efficient Ewald sum technique, and found that the cut-off radius technique slightly underestimated the efficiency of devices to an extent which depended upon the value of r_c. Hence the utility of the Ewald sum technique in application to OPV simulations is well demonstrated. Here we briefly discuss another technique that can be used to accurately calculate Coulombic interactions without excessive computational overhead.

The occupation probability of a site in a typical OPV simulation is typically 10^{-4}. Thus calculating everywhere the local potential due to Coulomb interactions, as occurs when using a potential array discussed above, is computationally wasteful. We can make significant savings by instead calculating the potential *only* where there is a possible change of occupation (i.e., the origin and possible destination sites). Practically this involves stepping through each of the carriers in the simulation, again excluding the carrier under consideration, and calculating the potential contribution of that charge and associated image charges to the site where one wants to calculate the potential. Calculations of the potential using this method thus scale like the carrier population rather than r_c^3, and usually result in orders of magnitude improvement in the simulation run-time while also improving accuracy[29] when compared to the potential array technique.

Returning to our present simulations of geminate separation efficiency, from all of the possible processes that can occur to a charge, we generate a random time-to-event using the following equation:

$$\tau = \frac{-\ln(X)}{w}. \tag{5}$$

Here X is a randomly generated number that is evenly distributed between 0 and 1, and w is the rate of the process being considered. The event with the shortest waiting time is chosen as the behavior for the carrier, and the time to that event is logged in the simulation queue. The simulation steps forward in time to execute the next event in the queue, shortening the time to other events by the corresponding amount, until either the carriers recombine or successfully separate, which here we define as having occurred when the carriers reach a separation of 25 nm. We note that this definition of the separation radius is somewhat arbitrary since one could argue that the carriers are not free until they are separated by more than the thermal capture radius ($\sim$16 nm) or infinity. However, since OPVs are of the order of $\sim$100 nm thick and domain sizes in optimized OPVs are of the order $\sim$10 nm, we view the separation radius of 25 nm to be a relevant length scale for OPV devices. It is noted that geminate and biomolecular recombination will compete in an OPV to some extent and consequently it is possible that geminate carriers which have separated by less than 25 nm,

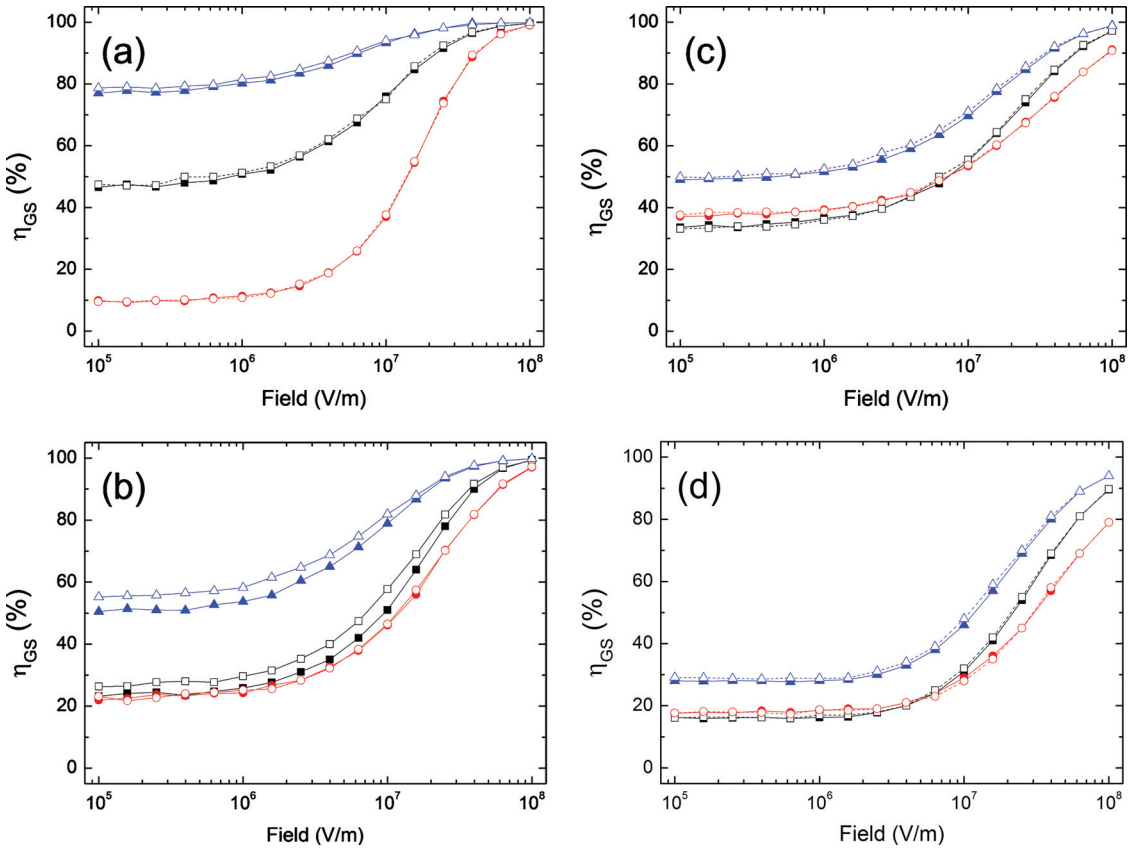

FIG. 1. Geminate separation efficiency, η_{GS}, as predicted by MMC for a bilayer when (a) $\sigma=0$ meV, (b) $\sigma=50$ meV, and (c) $\sigma=100$ meV. Black squares, red circles, and blue triangles correspond to $N_e=1$, 0 and 10, respectively, while all curves have $N_h=1$. Closed symbols and solid lines correspond to the FRM method, while open symbols and dashed lines to the exact method. Figure 1(d) shows η_{GS} for a $d=10$ nm blend when $\sigma=100$ meV.

and so would be considered Coulombically bound by the above definition, may recombine biomolecularly. However, since geminate recombination appears to be the major loss mechanism in some OPVs,[4,19–21] and that competition between geminate and bimolecular recombination ought to be viewed in a device context, we here consider geminate recombination as a standalone process. Returning to the simulations, at the end of each trial the energetic disorder is rechosen from the same distribution before being run again with a new geminate charge pair. The data shown here are the average of at least 10^5 trials.

We make another point here to comment on the importance of how hopping and recombination events are implemented within the model. Hopping is a process that is specific to the carrier under consideration, i.e., it is a one-carrier process, while recombination is a two-carrier process. This introduces a subtle but significant problem when one is calculating the behavior of the carriers. The carrier-specific nature of hopping obliges us to decide the behavior of the carrier on an individual basis. Hence if one is not careful, recombination may be double counted. To illustrate this problem, consider a geminate pair which has been created by a dissociating exciton. If one has structured the program in such a manner that all recombination processes and all hopping processes are considered for each carrier, the time to recombination will be calculated twice. Since the event at the top of the queue is chosen as the behavior for the carriers, there are two opportunities for recombination to be the fastest event rather than just one, which in turn makes recombination more likely. Thus one needs to ensure that for a pair of carriers the recombination behavior is calculated once only. Practically this can be achieved by simply "switching off" recombination for the first carrier prior to calculating the behavior of the second carrier with recombination "switched on." A benefit of the FRM becomes apparent here since carrier behavior is calculated one carrier at a time (apart from the initial injection of carrier pairs), and so the double counting of recombination does not occur. This would be rather difficult to achieve in an exact device model since for each recalculation of the carrier behaviors, which occur whenever a carrier hops or recombines, one would need to identify all of the carrier pairs and only calculate the time to recombination for each pair once.

III. RESULTS

The simulations reported in the main text were generated at the University of Durham, using a Monte Carlo code which was developed largely by the first author.[18,22] Some of these simulations were repeated at the University of Bath using a nominally identical Monte Carlo code[3,14] which was developed in isolation. The results of the Bath simulations, which correspond to Figs. 1(a)–1(c) and are shown in the supporting information,[36] are very similar to the Durham data reported in the main text as they reproduce all of the trends which we discuss in the forthcoming paragraphs. This

demonstrates the robustness of the technique and its portability to other research groups with use of papers freely available in the literature.

We begin by examining data corresponding to bilayer structures. Figures 1(a)–1(c) show geminate separation efficiency η_{GS} when $\sigma=0$, 50, and 100 meV, respectively, for a wide range of field F as predicted by both FRM and exact methods. For each value of energetic disorder considered we predict the behavior for three values of electron mobility factor $N_e=0$, 1, and 10 while we maintain $N_h=1$, which, respectively, correspond to one carrier being trapped, both carriers having nonzero equal mobility, and both carriers having finite but unequal mobility. The general behavior is the same for all curves, namely, that η_{GS} is saturated at small fields, increases as $\sim\exp(F/F_0)$ when F exceeds $\sim 4\times10^6$ V/m (where F_0 is a constant with units V/m), as opposed to linearly with field,[10] and saturates at $\sim$100% when F exceeds $\sim10^8$ V/m. Before we continue to discuss the difference between the FRM and exact methods, we will first discuss what such a comparison is expected to reveal by considering an electron-hole pair either side of a heterojunction. Within the FRM method, if the electrons were to move away from the hole, the hole would not be subject to the reduced Coulomb interaction that is a consequence of the receding electron until the hole moves and the new Coulombic environment is calculated. Therefore we would expect that the FRM would underestimate the separation efficiency when both carriers are mobile. By comparison, if one carrier is trapped (i.e., $N_e=0$) then the potential environment of the mobile carrier will never change and hence the FRM and exact methods should be coincident. Examining Figs. 1(a)–1(c) for $N_e=0$, we can see that the two models do coincide within the noise of the measurement, in agreement with our expectation. Now turning our attention to the cases examined where both carriers are mobile, $N_e=1$ and 10, we can see that the FRM model underestimates η_{GS}, again in agreement with our expectation. Additionally, we see that the difference between the models is not constant with field, and that the agreement between models improves with field. Figure 1(d) shows the separation efficiency predicted by the FRM and exact methods for a $d=10$ nm blend for the same range of mobilities as considered for Figs. 1(a)–1(c). As anticipated, the separation efficiency for a given mobility and field is lower for a blend than in a bilayer since the space available for separation and orientation of the interface to the field is less conducive to charge separation.[22] Furthermore, we see that the separation efficiency begins to increase at a higher field than for the bilayer device with a similar value of disorder. The agreement between the FRM and exact models for the blend is very similar to that shown for the bilayer device when using the same parameters.

To examine the agreement between models more closely, we calculate the average value of the data points shown in each of the Figs. 1(a)–1(c) for the FRM and exact methods, which we denote as $\langle\eta_{FRM}\rangle$ and $\langle\eta_{EX}\rangle$, respectively, which correspond to a "field average" value of η_{GS}. We then plot $\langle\eta_{FRM}\rangle-\langle\eta_{EX}\rangle$, which relates to the average difference between the two models, in Fig. 2 for each of the mobility combinations as a function of disorder. We also include in Fig. 2 corresponding data for $\sigma=25$, 75, and 150 meV, which we do not show in more detail for the sake of brevity.

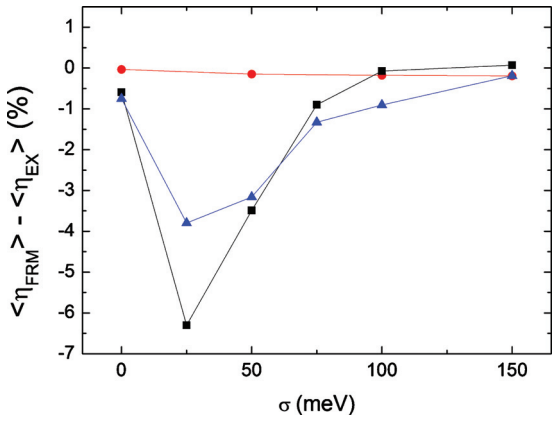

FIG. 2. The difference between field-average values of η_{GS} values predicted by FRM and exact methods, η_{FRM} and η_{EX}, respectively, over a range of values of energetic disorder σ. Black squares, red circles and blue triangles correspond to $N_e=0$, 1, and 10, respectively, while all curves have $N_h=1$.The range of energetic disorder values reported for conjugated polymers is rarely below 50 meV and most commonly around 100 meV.

Figure 2 shows that when both carriers are mobile ($N_e=1$, 10) the FRM method can underestimate η_{GS} to an extent that varies with energetic disorder. At zero disorder the FRM model underestimates η_{GS} by less than 1%, and with increasing σ, the agreement deteriorates up to $\sigma=25$ meV, where the FRM underestimates η_{GS} by $\sim$6.5%, before gradually improving until the FRM and exact methods agree to better than 1% when $\sigma\geq100$ meV. The agreement/disagreement between the models appears to be relatively insensitive to the magnitudes of the carrier mobilities provided that both carriers are mobile. While a peak disagreement of $\sim$6.5% may seem serious, two important caveats should be borne in mind. First, the agreement between the models improves with the electric field [see Figs. 1(a)–1(c)], and thus at short circuit and at the maximum power point of an OPV, the agreement between the FRM and exact methods will be better than the field average values shown in Fig. 2. Second, and most importantly, the range of disorder reported for technologically relevant conjugated polymers, such as polyfluorenes,[33,34,37] polythiophenes,[38–40] and alkoxy poly(phenylene vinylene) derivatives,[38,41,42] is generally $\sigma>50$ meV. In this regime the agreement between the computationally less expensive FRM and exact method is better than 2%. This is a key result.

It is interesting to understand the reason for the σ dependence of the agreement between the FRM and exact models even though there is good agreement over the range of interest. When $\sigma=0$, the disagreement between models is $\sim$1%, which increases rapidly to a peak when $\sigma\sim25$ meV, before gradually reducing as σ increases further. To explain this, we will first consider the effect of introducing disorder to the separation process. In a bilayer geometry, a carrier can escape its partner's influence by following any of the routes in the hemisphere of material that transports that charge carrier. When disorder is introduced, some of these routes will become more difficult to follow due to unfavorable combinations of the local energetic disorder. When disorder is in-

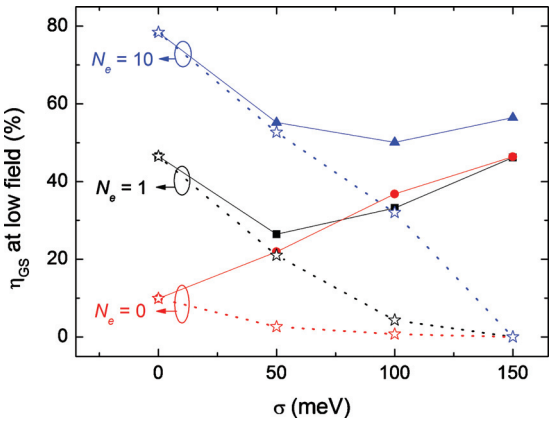

FIG. 3. Low-field dissociation probability η_{GS} as a function of energetic disorder σ as predicted by the exact model when carriers are injected at random into the density of states (solid) and when the carriers are injected at a more equilibrated energy of $-\sigma^2/2kT$ (open).

creased, the number of routes to separation is reduced due to the undulating potential landscape, in much the same way a blend morphology reduces the number of routes to separation.[22] Thus increasing σ carries with it an implicit reliance on progressively fewer routes to successful separation. We speculate that the reliance on fewer likely routes to separation when σ increases makes the process of predicting η_{GS} more sensitive to errors in the way in which electrostatics are treated, thus further reducing $\langle \eta_{FRM} \rangle$ as compared to $\langle \eta_{EX} \rangle$ when σ increases. However, when we approach the limt of large σ, the the probability of carriers becoming trapped increases. Since it has been shown that when one carrier is trapped ($N_e=0$) that the the FRM and exact models coincide (Fig. 2), we further speculate that good agreement between the FRM and exact models in the limit of large σ is due to charge trapping. These two mechanisms, involving the fewer likely routes to separation (which reduces $\langle \eta_{FRM} \rangle$ with increasing σ) and the increased probability of charge trapping (which reduces the difference between $\langle \eta_{FRM} \rangle$ and $\langle \eta_{EX} \rangle$ with increasing σ), though speculative, could explain the data shown in Fig. 2.

We tested these proposed mechanisms further by repeating the simulations for the $\sigma=50$ meV bilayer with spatially correlated energetic disorder in the manner of Gartstein and Conwell[43] with a correlation range of 1 nm. The effect of correlating disorder is to reduce the probability of isolated traps or potential barriers, thus reducing the effect of both of the mechanisms we describe above. We find that the agreement between the FRM and exact model "field average" improves to being better than 2% difference for $N_e=1$ and 10, in comparison to a greater than 3% disagreement shown for when energetic disorder is spatially random (as shown in Fig. 2). These data show that the disagreement between the FRM and exact models is sensitive to the spatial arrangement of energetic disorder, which is consistent with our proposed explanation of the disagreement between the two models.

The low-field values of η_{GS}, as predicted by the exact model, are shown to have an unexpected dependence on σ that is replotted in a more convenient form in Fig. 3. One might expect that increasing the value of σ, and thus reducing the equilibrium mobility, would result in a monotonic reduction in the low-field value of η_{GS}. However, for the current simulations show that when both carriers are mobile the low-field η_{GS} reduces and then increases with increasing σ, while when one carrier is mobile the low-field η_{GS} monotonically increases. It is important to understand these unexpected results since low-field charge separation can play a part in determining the photocurrent under forward bias, and thus the open circuit voltage of OPVs. We explain the trends shown in Fig. 3 by equilibration effects. When disorder is increased, we also increase the degree of energy available to a carrier early in its attempt to separate since the initial energy of the carrier is that of the site it was created. When one carrier is trapped, the mobile carrier can use this energy to its best advantage since the opposite carrier will not "follow" the mobile charge in the plane of the heterojunction.[3,22]

However, when both carriers are mobile, any initial separation obtained by a carrier from initial energy can be nullified by the opposite carrier "following" it in the plane of the heterojunction. Thus, one must provide more initial enery (i.e., large σ) to see an improvement in separation efficiency when both carriers are mobile compared to when only one carrier is mobile (Fig. 3). To confirm these assertions, the above simulations were repeated while setting the initial energy of the charge carriers to be a fraction of the equilibrium energy,[44] $\sigma^2/2kT$, and are plotted as open symbols on Fig. 3. These data recover the monotonic decrease in η_{GS} with increasing σ that was originally expected.

IV. SUMMARY

Here we have evaluated the accuracy of a commonly used approximation in MMC models, the FRM, in the prediction of geminate separation efficiency over a wide range of values of energetic disorder, mobility, and electric fields that are relevant for OPVs. It is shown that for most OPV materials in which $\sigma \sim 100$ meV the separation probability of geminate charges predicted by the FRM model agrees with the exact method to within 2%. This shows that the computational burden of MMC models can in most cases be reduced with the use of the FRM method without significantly affecting simulation accuracy. Outside the range of values of energetic disorder which are of interest in most conjugated polymers of interest (25 meV $\leq \sigma \leq$ 50 meV), the agreement between the FRM and exact method is shown to be worse, reaching a peak disagreement of 6.5%. The disorder dependence of the agreement between models is explained in terms of the disorder dependence of the number of available routes to separation and the disorder dependence of trapping. Additionally, we demonstrate the strong effect that the initial energy of charges has upon the subsequent separation behavior.

ACKNOWLEDGMENTS

This work was supported by the European Commission FP-6 program MODECOM (Grant No. NMP-CT-2006-016434). R.G.E.K. thanks the UK Engineering and Physical Sciences Research Council for a studentship. Simulations

were carried out on the Durham University Hamilton Supercomputing cluster and the University of Bath High Performance Cluster "Aquila."

[1] G. Yu, J. Gao, J. C. Hummelen, F. Wudl, and A. J. Heeger, Science **270**, 1789 (1995).
[2] J. J. M. Halls, C. A. Walsh, N. C. Greenham, E. A. Marseglia, R. H. Friend, S. C. Moratti, and A. B. Holmes, Nature (London) **376**, 498 (1995).
[3] R. G. E. Kimber, A. B. Walker, G. E. Schroder-Turk, and D. J. Cleaver, Phys. Chem. Chem. Phys. **12**, 844 (2010).
[4] C. R. McNeill, S. Westenhoff, C. Groves, R. H. Friend, and N. C. Greenham, J. Phys. Chem. C **111**, 19153 (2007).
[5] S. R. Scully and M. D. McGehee, J. Appl. Phys. **100**, 034907 (2006).
[6] A. J. Moulé and K. Meerholz, Adv. Funct. Mater. **19**, 3028 (2009).
[7] C. R. McNeill and N. C. Greenham, Adv. Mater. **21**, 3840 (2009).
[8] C. Groves, O. G. Reid, and D. S. Ginger, Acc. Chem. Res. **43**, 612 (2010).
[9] J. Nelson, J. J. Kwiatkowski, J. Kirkpatrick, and J. M. Frost, Acc. Chem. Res. **42**, 1768 (2009).
[10] R. A. Marsh, C. R. McNeill, A. Abrusci, A. R. Campbell, and R. H. Friend, Nano Lett. **8**, 1393 (2008).
[11] L. J. A. Koster, E. C. P. Smits, V. D. Mihailetchi, and P. W. M. Blom, Phys. Rev. B **72**, 085205 (2005).
[12] J. J. M. van der Holst, M. A. Uijttewaal, R. Balasubramanian, R. Coehoorn, P. A. Bobbert, G. A. de Wijs, and R. A. de Groot, Phys. Rev. B **79**, 085203 (2009).
[13] S. Athanasopoulos, J. Kirkpatrick, D. Martinez, J. M. Frost, C. M. Foden, A. B. Walker, and J. Nelson, Nano Lett. **7**, 1785 (2007).
[14] P. K. Watkins, A. B. Walker, and G. L. B. Verschoor, Nano Lett. **5**, 1814 (2005).
[15] R. A. Marsh, C. Groves, and N. C. Greenham, J. Appl. Phys. **101**, 083509 (2007).
[16] F. Yang and S. R. Forrest, ACS Nano **2**, 1022 (2008).
[17] L. Y. Meng, Y. Shang, Q. K. Li, Y. F. Li, X. W. Zhan, Z. G. Shuai, R. G. E. Kimber, and A. B. Walker, J. Phys. Chem. B **114**, 36 (2010).
[18] C. Groves, J. C. Blakesley, and N. C. Greenham, Nano Lett. **10**, 1063 (2010).
[19] A. Gonzalez-Rabade, A. C. Morteani, and R. H. Friend, Adv. Mater. **21**, 3924 (2009).
[20] R. A. Marsh, J. M. Hodgkiss, and R. H. Friend, Adv. Mater. **22**, 3672 (2010).
[21] D. Veldman, O. Ipek, S. C. J. Meskers, J. Sweelssen, M. M. Koetse, S. C. Veenstra, J. M. Kroon, S. S. van Bavel, J. Loos, and R. A. J. Janssen, J. Am. Chem. Soc. **130**, 7721 (2008).
[22] C. Groves, R. A. Marsh, and N. C. Greenham, J. Chem. Phys. **129**, 114903 (2008).
[23] U. Albrecht and H. Bassler, Chem. Phys. Lett. **235**, 389 (1995).
[24] T. Offermans, S. C. J. Meskers, and R. A. J. Janssen, Chem. Phys. **308**, 125 (2005).
[25] C. Deibel, T. Strobel, and V. Dyakonov, Phys. Rev. Lett. **103**, 036402 (2009).
[26] C. Groves and N. C. Greenham, Phys. Rev. B **78**, 155205 (2008).
[27] C. Groves, L. J. A. Koster, and N. C. Greenham, J. Appl. Phys. **105**, 094510 (2009).
[28] J. J. Lukkien, J. P. L. Segers, P. A. J. Hilbers, R. J. Gelten, and A. P. J. Jansen, Phys. Rev. E **58**, 2598 (1998).
[29] M. Casalegno, G. Raos, and R. Po, J. Chem. Phys. **132**, 094705 (2010).
[30] P. Peumans, S. Uchida, and S. R. Forrest, Nature (London) **425**, 158 (2003).
[31] J. M. Frost, F. Cheynis, S. M. Tuladhar, and J. Nelson, Nano Lett. **6**, 1674 (2006).
[32] I. C. Henderson and N. Clarke, Macromolecules **37**, 1952 (2004).
[33] J. C. Blakesley, H. S. Clubb, and N. C. Greenham, Phys. Rev. B **81**, 045210 (2010).
[34] R. U. A. Khan, D. Poplavskyy, T. Kreouzis, and D. D. C. Bradley, Phys. Rev. B **75**, 035215 (2007).
[35] J. K. Grey, D. Y. Kim, C. L. Donley, W. L. Miller, J. S. Kim, C. Silva, R. H. Friend, and P. F. Barbara, J. Phys. Chem. B **110**, 18898 (2006).
[36] See supplementary material at http://dx.doi.org/10.1063/1.3483603 for corresponding data from Bath University simulations.
[37] T. Kreouzis, D. Poplavskyy, S. M. Tuladhar, M. Campoy-Quiles, J. Nelson, A. J. Campbell, and D. D. C. Bradley, Phys. Rev. B **73**, 235201 (2006).
[38] C. Tanase, E. J. Meijer, P. W. M. Blom, and D. M. de Leeuw, Phys. Rev. Lett. **91**, 216601 (2003).
[39] R. J. Kline, M. D. McGehee, E. N. Kadnikova, J. Liu, J. M. J. Frechet, and M. F. Toney, Macromolecules **38**, 3312 (2005).
[40] A. J. Mozer and N. S. Sariciftci, Chem. Phys. Lett. **389**, 438 (2004).
[41] W. F. Pasveer, J. Cottaar, C. Tanase, R. Coehoorn, P. A. Bobbert, P. W. M. Blom, D. M. de Leeuw, and M. A. J. Michels, Phys. Rev. Lett. **94**, 206601 (2005).
[42] M. Bouhassoune, S. L. M. v. Mensfoort, P. A. Bobbert, and R. Coehoorn, Org. Electron. **10**, 437 (2009).
[43] Y. N. Gartstein and E. M. Conwell, Chem. Phys. Lett. **245**, 351 (1995).
[44] H. Bässler, Phys. Status Solidi B **175**, 15 (1993).